American Journal of Materials Science 2014, 4(2): 64-73
DOI: 10.5923/j.materials.20140402.03

Surfactant Assisted Synthesis of Copper Oxide (CuO) Leaf-like Nanostructures for Electrochemical Applications

A. Bello[1], D. Dodoo-Arhin[1,2,*], K. Makgopa[3], M. Fabiane[1], N. Manyala[1]

[1]Department of Physics, SARCHI Chair in Carbon Technology and Materials, University of Pretoria, Pretoria 0028, South Africa
[2]Department of Material Science and Engineering, University of Ghana, Legon-Accra, Ghana
[3]Department of Chemistry, University of Pretoria, Pretoria 0002, South Africa

Abstract Three different copper oxide (CuO) leaf-like nanostructures have been synthesised by micelles micro emulsion method using a surfactant of copper dodecyl sulphate ($Cu(DS)_2$) by varying the concentration of sodium hydroxide (NaOH). This study was carried out to investigate the effect of NaOH concentration on the stability, crystalline domain and pseudocapacitance behaviour of the leaf-like nanostructures. The samples were characterized by X-ray diffraction (XRD), thermogravimetry analysis (TGA), Raman spectroscopy, Fourier-Transform Infrared (FTIR), scanning electron microscopy (SEM) and Transmission electron microscopy (TEM). It was observed that the crystalline domain size (12 nm-18 nm) and size distribution of the as-synthesized nanocrystals decreases with increasing concentration of NaOH. The interactions mechanism and formation of the leaf-like structure have been elucidated and correlated with various analytical techniques. The domain size and NaOH concentration tend to influence the charge transfer resistance.

Keywords Chemical synthesis, Nanostructures, Powder diffraction, Semiconductors

1. Introduction

In recent years, nanostructured semiconducting materials have stimulated intensive research activities due to their exceptional properties arising from their high surface/ volume ratio and nanoscale quantum confinement effects. Copper oxides are useful reference systems for the study of complex cuprates, most of which show high-temperature superconductivity (high-T_c). This phenomenon has been attributed to a Jahn-Teller distortion in a symmetric divalent copper monoxide structure which introduces a strong electron-phonon interaction leading to the superconductivity [1, 2]. Amongst the mono oxides of 3d transition series, cupric oxide (CuO) is unique due to it planar square coordination in a monoclinic structure. The copper forms four coplanar bonds with oxygen which itself is coordinated by four copper atoms in a distorted tetrahedral environment. The monoclinic (space group: $C2/c$-C_{2h}^6, 15) possesses four units formula in its crystallographic unit cell with lattice constants of a=0.46837 nm, b=0.34226 nm, c=0.51288 nm, β=99.54º. The positions of the atoms in the cell are: **Cu(4c):** $1:\left(\frac{1}{4},\frac{1}{4},0\right)$, $2:\left(\frac{3}{4},\frac{1}{4},\frac{1}{2}\right)$; **O(4e)**: $3:\left(0,y,\frac{1}{4}\right)$, $4:\left(0,\bar{y},\frac{3}{4}\right)$, where y=0.4184; with equivalent positions of (0,0,0) and $\left(\frac{1}{2},\frac{1}{2},0\right)$. The three dimensional crystal structure of the CuO is built from the two sets of chains $^1_\infty\left[CuO_{4/2}\right]$ directed along [110] and staggered along [001] [3, 4].

CuO is p-type semiconductor with narrow and indirect energy band-gap of 1.2-1.8 eV, [5, 6]; has attracted a lot of research interest due to its unique properties such as high catalytic activity, easy synthesis route, environmentally friendly nature and variable morphologies at the nanoscale. It has found applications in electrochemistry as electrode material for lithium-ion batteries and electrochemical capacitors, solar energy systems, heterogeneous catalysts and selective gas sensors [7, 8].

Several strategies have been used for production of CuO nanostructures with different morphologies [9–12]. Structures such nanobelts [13], nanowires, nanorods, nanotubes [14–18], nanoribbon [19, 20], nanoplatlete [21] dumbbell [22] and nanoparticles [16]. The morphologies of CuO nanostructures have been shown to have effects on the optical, semiconducting, and piezoelectric properties. The different procedures used for the production of CuO nanostructure include sonochemical deposition [23], high temperature synthesis [24], chemical vapour deposition [25], double-jet precipitation [26], microemulsion synthesis [27] etc.

Microemulsion is a self-assembly technique driven by

* Corresponding author:
ddarhin@yahoo.com (D. Dodoo-Arhin)
Published online at http://journal.sapub.org/materials

factors such as surface tension, capillary effects, electric and magnetic forces, and hydrophobic-hydrophilic interactions. It is known to be an effective approach to forming a wide variety of motifs, otherwise impossible under equilibrium conditions [28]. The fundamental challenge with this technique is the accurate control over the final CuO nanostructures with specific uniform morphologies. Hence, a good analytical technique to characterize the size and size distribution of the crystalline domains is very important. Techniques such as TEM and XRD usually consider the average size and are limited to the analysis of a determinate number of particles. The state of the art alternative is the analysis of the XRD data by full pattern methods such as the Whole Powder Pattern Modelling (WPPM) [29], that allows interpretation of the whole diffraction pattern in terms of physical models for the broadening sources (instrumental and sample) directly refined on the experimental data, with no arbitrary assumptions on the diffraction patterns.

In this work, we present results of a thermal and surfactant assisted self-assembly synthesis of copper oxide leaf-like nanostructure. The obtained nanocrystals have been characterized by XRD, SEM, TEM, FTIR, and Raman spectroscopy. The resulting CuO samples were investigated as a potential electrode material for electrochemical applications.

2. Experimental

2.1. Materials and Chemicals

Copper chloride dihydrate ($CuCl_2$•$2H_2O$, Merck 97%), ethanol (purity Merck 98%), sodium hydroxide (NaOH, Merck 98%) anionic surfactant (sodium dodecyl sulphate SDS, Sigma Aldrich) were used as CuO precursors. All chemicals were used as received. Deionized water was used throughout the preparations.

2.2. CuO Synthesis

A stable stock solution of 8.0 mM copper dodecyl sulphate ($Cu(DS)_2$) was prepared by mixing sodium dodecyl sulphate surfactant (SDS) and copper chloride dihydrate ($CuCl_2$•$2H_2O$) flakes/crystals in a beaker containing 40 ml of deionized water and stirred for about 10 minutes at 50ºC to ensure complete dissolution. The final solution was filtered to separate any filtrate residue. This dark greenish-blue solution serves as source (Cu^{2+}) for synthesis of CuO [7].

In a typical synthesis, three batches of 40 ml solution each were made in a 80 ml graduated borosilicate glass bottle, closed with a polypropylene cap (to limit evaporation) by adding 1 ml of the $Cu(DS)_2$ aqueous stock solution into a 37 ml deionized water; leads to the formation of a homogeneous and transparent sky-blue microemulsion without any form of precipitate. Afterwards, 2 ml of variable aliquots (1.5 M, 2.0 M and 2.5 M, according to Table 1) of NaOH solution was added to the dispersion under constant magnetic stirring leading to a deep blue solution without precipitation. The mixture was then heated at 80°C under constant magnetic stirring at 200 rpm for 4 hours. The mixture gradually turned into a dark brown-black precipitate which was cooled and later centrifuged at 6000 rpm for 10 minutes to separate the particles from the suspension.

Table 1. Experimental parameters and microstructure data

Sample	NaOH Conc. (M)	Av. size (nm)	a (nm)	b (nm)	c (nm)	β (degrees)
CuO-1.5	1.5	18.2	0.4696	0.3439	0.5130	99.62
CuO-2.0	2.0	13.9	0.4688	0.3444	0.5130	99.53
CuO-2.5	2.5	12.6	0.4690	0.3439	0.5126	99.55

To remove the surfactant phase possibly attached to the surface of the particles, 20 ml ethanol and 20 ml deionised water was added to the precipitate sonicated and centrifuged at 6000 rpm for 10 minutes. The particles were further washed several times with deionised water and dried at 60°C. Each batch was produced at least 3 times to guarantee the reproducibility of the result.

The working electrodes for electrochemical evaluation were prepared by mixing 80 wt. % CuO, 10 wt. % carbon black (to improve the conductivity), 10 wt. % Polyvinylidene (PVDF) and homogenized in an N-methyl pyrrolidone (NMP) solvent to form slurry. The slurry was pasted on a Ni foam current collector and then dried for 12 hours in an electric oven at 80.0°C to ensure complete evaporation of N-methyl pyrrolidone (NMP).

2.3. Characterizations

X-ray diffraction (XRD) patterns of the sample were collected on an XPERT-PRO diffractometer (PANalytical BV, Netherlands) with theta/theta geometry, operating a cobalt tube at 35 kV and 50 mA. The goniometer is equipped with automatic divergence Slit and a PW3064 spinner stage. The instrumental resolution function was characterized with the NIST SRM 660a (LaB_6) standard. All peak profiles of the LaB_6 phase were simultaneously fitted with symmetrical pseudo-Voigt functions whose width and shape were constrained according to the Caglioti et al. formulae [30]. The XRD patterns of all specimens were recorded in the 40.0°- 80° 2θ range with a step size of 0.017° and a counting time of 15.240 second per step. Qualitative phase analysis of samples was conducted using the X'pert Highscore Plus search match software. Microstructural analysis of the data was implemented by employing the Whole Powder Pattern Modelling (WPPM) method [29], incorporated in the PM2K software [31].

Fourier-Transform Infrared (FTIR) spectra were recorded on a Vertex 70v (Bruker) spectrometer in the 4000-400 cm^{-1} range with 4 cm-1 resolution. Spectra were recorded and analysed with the Opus software. Raman spectroscopy data were collected on a Jobin Yvon Horiba TX 6400 micro-Raman spectrometer equipped with a triple monochromator system and LabSpec (Ver. 5.78.24) analytical software. All the samples were analysed with a

514 nm Argon excitation laser through an X 50 objective with acquisition time of 120 seconds and a resolution of 2 cm^{-1}. A high resolution Zeiss Ultra plus 55 scanning electron microscope (SEM) operated at 2.0 KV was used for surface morphological investigations of the as-produced particles. Further microstructure analysis was made on a JEOL JEM-2100F transmission electron microscope (TEM) operated at 200 KV. Standard DSC-TGA experiment was performed on a SDT Q600 (V20.9 Build 20) instrument. The samples were place in an alumina crucible and heated in air at a temperature rate of 10ºC/minute from room temperature to 800ºC. Finally electrochemical measurements cyclic voltammetry (CV), galvanostatic charge-discharge (CD) and electrochemical impedance spectroscopy (EIS) were performed using an Autolab PGSTAT 302 workstation (ECO-CHEMIE) driven by a GPES software. The CuO paste on a nickel foam served as the working electrode, glassy carbon plate as the counter electrode, Ag/AgCl (3 M KCl) served as the reference electrode and 2 M KOH aqueous electrolyte was used.

3. Results and Discussion

3.1. Synthesis Reaction Mechanism

In aqueous solution, $CuCl_2$ dissociates into $[Cu(H_2O)_6]^{2+}$ ions (responsible for the sky blue colouring) and Cl^- anions: will partially coordinate with copper ions In $[Cu(H_2O)_6]^{2+}$, the six water molecules completely surround the Cu^{2+} ion, shielding it. The accessibility of the copper ion in this complex is highly favoured, as the coordination with water is weak [32]. At temperatures higher than room temperature, CuO can be formed through the following scheme [33]:

$$Cu^{+}(aq)+2OH^{-}(aq) \rightarrow Cu(OH)_2(aq) \quad (1)$$

$$Cu(OH)_2(aq) + 2OH^{-}(aq) \rightarrow Cu(OH)_4^{2-}(aq) \longleftrightarrow CuO(s) + 2OH^{-}(aq) + H_2O \quad (2)$$

Nanoparticles formed inside reverse micelles undergo further growth or aggregation yielding particles "larger" than their initial nanodroplets which may result in a multimodal distribution. Due to the solvating action when copper salt is dissolved in water, four water molecules surround the Cu^{2+} to form a square structure $(Cu(OH)_4^{2-})$ and the other two water molecules are located on its axis. According to the anionic coordination polyhedra theoretical model [34, 35], cations exist in the form of complexes whose ligands are OH^- ions in an aqueous solution: the complex whose coordination numbers are equal to that of the crystal, forms the growth unit. Moreover, the formation of growth units and the incorporation of the growth units into the crystal nucleus are induced by a dehydration reaction.

In the SDS-Copper aqueous solution, the hydrophilic group of the surfactant points to the outer surface of the capsule surrounding the water pool, while the hydrophobic ends points inward due to the electrostatic interaction of the sulfonic groups of the SDS and the Cu^{2+} ions. The outer surface of the hydrophilic end is occupied by numerous Cu^{2+} ions. Upon addition of the varied concentrations of NaOH, the hydroxyl groups react to form dodecyl sulphate copper hydroxide ion $(DSCu(OH)_2^{4-})$ nuclei which form active sites to generate DS[$Cu(OH)_2$]n structures. Accordingly, the growth units for the CuO nanocrystals are therefore considered to be $(Cu(OH)_6^{4-})$, which is a coordinating octahedron in the NaOH solution. In this case, four OH^- ions are arranged on a planar square, and the other two OH^- ions are located on a perpendicular axis.

The binding energies of the two OH^- ions located on the octahedron axis are known to be lower than those OH^- groups located on the plane axis [36]. In view of this, the two OH^- ions located at the axis are easily replaced and dehydrated to form CuO nanocrystallites; hence the growth rate along the axes is higher than in the plane. The growth mechanism and formation of different shapes of CuO nanocrystals (e.g. nanorods, nanobelts, nanowires, etc) can therefore be explained with this difference in growth rates along various directions. The reaction temperature as in such synthesis can play an important role in the crystal growth process. In more detail, the reactions leading to the formation of CuO can be summarised into:

$$Cu^{2+}Cl^{-}(aq)+2Na^{+}OH^{-}(aq) \longrightarrow Cu(OH)_2(aq) + 2NaCl(aq) \quad (3)$$

$$Cu(OH)_2(aq) + 2OH^{-}(aq) \longrightarrow \left[Cu(OH)_4\right]^{2-}(aq) \quad (4)$$

$$\left[Cu(OH)_4\right]^{2-}(aq) \xrightarrow{heat} CuO_{(s)} + 2OH^{-}(aq) + H_2O \quad (5)$$

At low temperatures, the hydroxyl groups of the $(Cu(OH)_6^{4-})$ complex (produced when NaOH is added) might form hydrogen bonds by interconnection: the directional growth would then be inhibited, leading to the formation of irregularly shaped nanocrystals [37, 38]. However, at higher temperatures close to room temperature ($T \leq 25°C$) only small quantities of hydrogen bonds are destroyed. The residual hydrogen bonds may still lead to the formation of structures with mixed morphologies. When the reaction temperature is increased ($25°C < T < 100°C$), there is a corresponding increase in the nucleation and growth rates as well as the destruction of more hydrogen bonds. In our case, the reaction temperature has been chosen to be 80°C to prevent evaporation of the water. Further investigation on the effect of reaction temperature and time on the particle size, size distribution, morphology and the surfactant breaking point boundary conditions of the SDS will lead to a better understanding of the growth mechanism of the as-produced CuO nanostructures.

In the synthesis, reactions (3) and (4) take place within micelles of the microemulsion. The microemulsion droplets act as the nanoreactors to produce the dissolved DS-$Cu(OH)_2$ nanocrystals. Based on its structural features and specific interactions of the Cu^{2+} ions with ligands in the solution, DS-$Cu(OH)_2$ tends to form a wire-like structure. This structure has been shown to consist of oblate chains of

$Cu(OH)_2$ in the (001) planes and oriented along the [100] direction: a feature characteristic of the square-planar coordinated Cu^{2+} ions [39]. The surfactant molecules adhere to the surface of the final nanoparticles which serve as a protective layer to prevent fusion of the droplets as a result of collisions [40, 41]. These can be removed by washing with ethanol and deionised water.

3.2. X-Ray Diffraction Analysis and Electron Microscopy

Figure 1a reveal that all the diffraction peaks can be indexed to the monoclinic CuO structure (JCPDS, file No. 80-1917) with negligible traces of residual $Cu(OH)_2$ which could be due to reaction time. The broadening of the diffraction peaks suggests a nanometre scale crystalline domain size. Microstructure analysis was performed on the patterns using the Whole Powder Pattern Modelling approach, which directly connects a physical model for the microstructure with the diffraction pattern, allowing an extraction of microstructure parameters without recurring arbitrary peak shapes to fit each diffraction peak. Figure 1b shows the typical diffraction pattern of CuO-1.5 modelled using the WPPM.

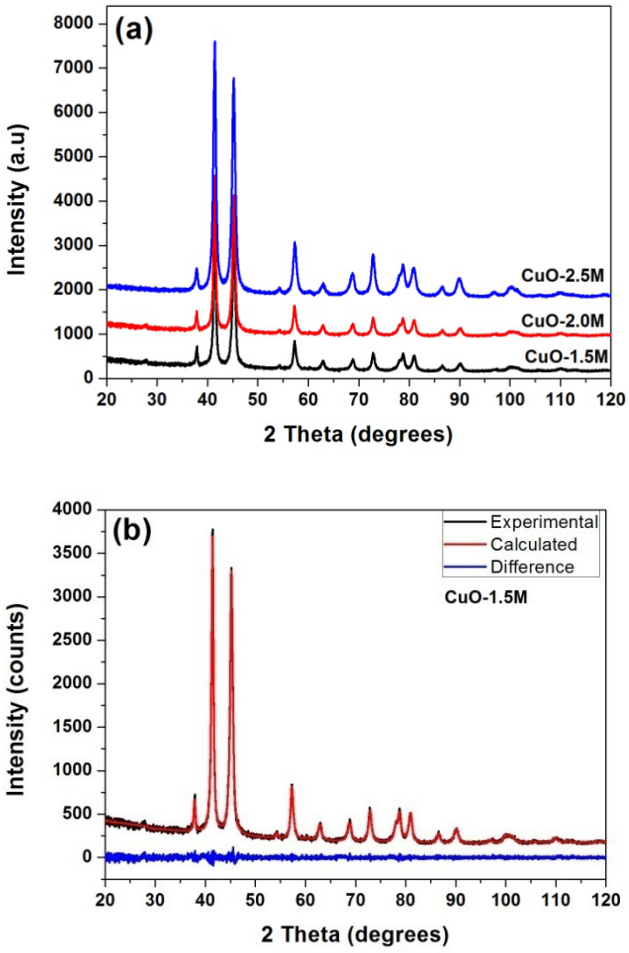

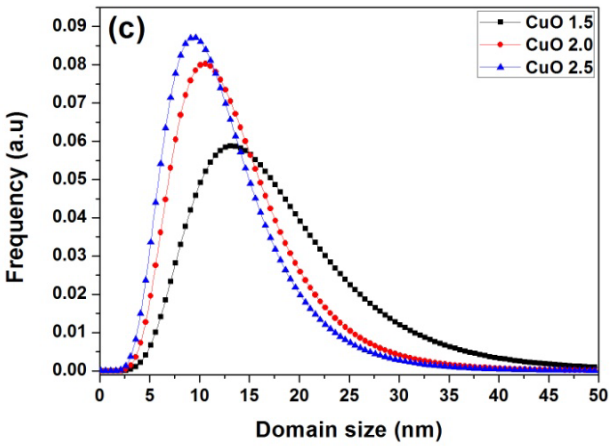

Figure 1. (a) X-ray diffraction pattern of the as-synthesised CuO nanostructures. (b) CuO-1.5 modelled using the WPPM, and (c) lognormal distribution of aligned spherical domains

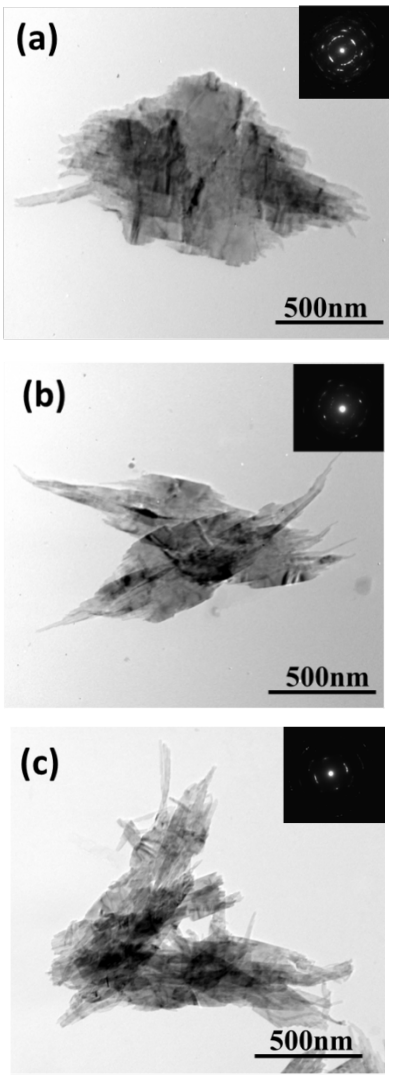

Figure 2. **(a-c)** TEM images of CuO leaf-like nanostructures

The modelling was carried out by assuming the presence of a lognormal distribution (figure1c) of aligned spherical domains. The almost featureless nature of the residual line figure 1b indicates a good agreement between experimental data and model which also suggests that the shape assumption is right for the domains investigated. The average crystallite size ranges from ~8 nm (CuO-2.5) to~16 nm (CuO-1.5): a clear correlation between domain size and NaOH concentration inside the micelles.

The TEM images in figure 2 (a-c) indicate the synthesis of leaf-like nanostructures for all the conditions investigated. It seems that the leaf-like structure comprises small spherical particles that have been self-aligned to form rods in a leaf-like morphology. This is consistent with earlier explanation of the directional growth of CuO nanocrystals along the axis. Insert to figures 2 (a-c) shows the selected area electron diffraction (SAED) of the CuO samples produce revealing that it is polycrystalline in nature.

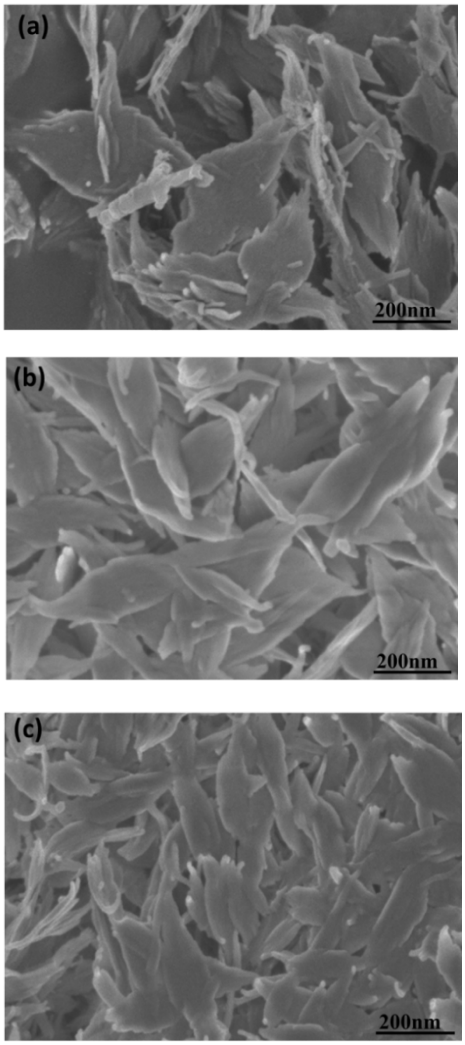

Figure 3. SEM micrograph of the as-synthesised CuO leaf-like nanostructures

The similar consistent features are found in the SEM micrograph figure 3 showing the leaf-like structures. This is also an indication that particles are directionally aligned along the rods but have no crystallographic relationship (i.e. a proper epitaxy did not occur).

3.3. ATR-FTIR and Raman Spectroscopy

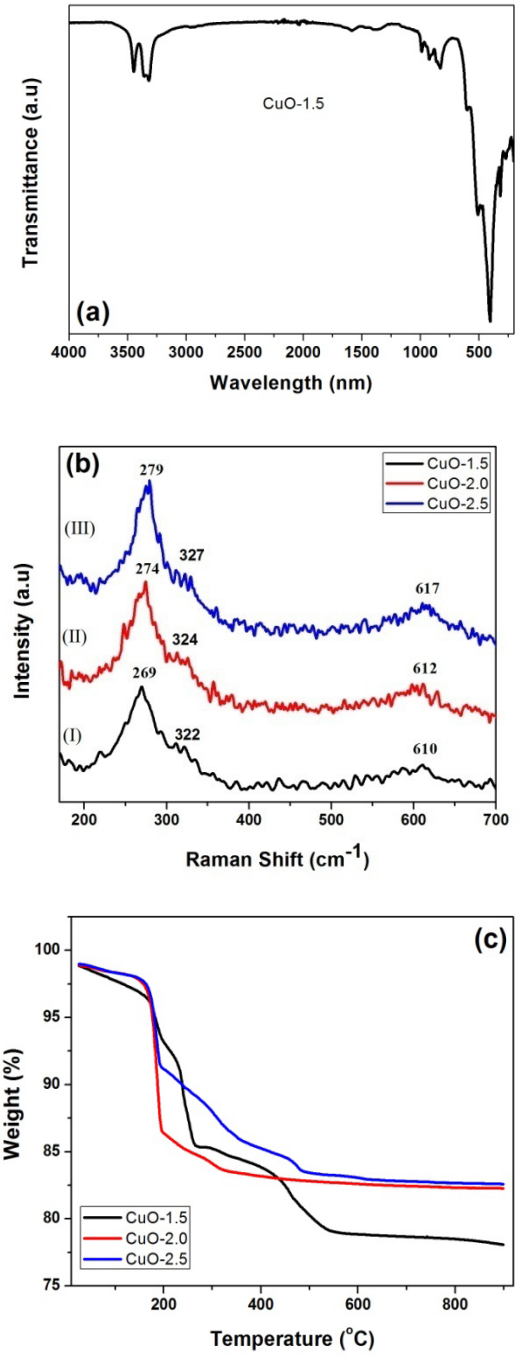

Figure 4. (a) Representative FTIR spectrum (CuO-1.5), (b) Raman spectra and (c) thermal analysis of the as-synthesised CuO nanocrystals

The representative FTIR spectra (figure 4a) of the synthesized CuO nanostructures (CuO-1.5) show three characteristic infrared peaks around 403, 508, and 602 cm^{-1} which could be attributed to the monoclinic structure of CuO [42]. The absorption bands at 602 cm^{-1} and 508 cm^{-1} are attributed to the Cu-O stretching along the direction, and the 403 cm^{-1} to the Cu-O stretching along [43]. No active

bands from Cu_2O or impurities were observed, thus, indicating the formation of pure CuO sample from FTIR study. There was no significant observation of shifts in the peaks with increase or decrease in crystallite domain size

Hence, Raman spectroscopy was used as a complementary tool to further probe the structural effect of the as-grown CuO nanocrystals. As shown in figure 4b, the Raman spectra show three broad characteristic peaks for all the samples under study. Group theory and semi-empirical calculations of the vibrational properties of CuO indicate that it possesses 12 phonon branches owing to the four atoms in the primitive cell. They comprise three acoustic modes (A_u + $2B_u$) and nine (9) zone-center optical phonon modes with symmetries of $4A_u+5B_u+A_g+2B_g$; however, only three symmetry modes ($Ag+2B_g$) are Raman active located at peak positions of 298 (A_g), 345($2B_g$) and 632 cm^{-1} ($2B_g$) [44, 45].

The other remaining six ($3A_u+3B_u$) are IR active [42]. In the A_g and B_g Raman modes, only the oxygen atoms move, with displacements in the b-direction for A_g and perpendicular to the b-axis for B_g modes. The infrared active modes involve the motion of both the O and the Cu atoms. The induced dipole moment is along the b-axis for the A_u modes and perpendicular to it for the B_u modes. From figure 4b, peak positions of the samples are observed as: CuO-1.5 (269 cm^{-1}, 322 cm^{-1} and 610 cm^{-1}); CuO-2.0 (274 cm^{-1},324 cm^{-1} and 612 cm^{-1}); CuO-2.5 (279 cm^{-1}, 327 cm^{-1} and 617 cm^{-1}) respectively. The peak sharpness and peak position increases slightly to higher wave numbers with increase in NaOH concentration and also in the crystallites sizes as observed in the XRD analysis. It is worth noting that the Raman intensity (I_v) of nanocrystals (spherical) is a superposition of the weighted Lorentzian contributions over the whole Brilloun zone. This is mathematically represented in equation (6). Where ν(φ) is the phonon dispersion factor, Γ_0 is the natural full line width and C(0,φ) is the Fourier coefficient of the phonon confinement function.

$$I(\upsilon)=\frac{\left|C(0,\varphi)\right|^2}{\left[\upsilon-\upsilon(\varphi)\right]^2+\left(\Gamma_0/2\right)^2}d^3\varphi \qquad (6)$$

The Fourier coefficient of the phonon confinement function is often taken as in equation (7), where d is the average size of the nanocrystals

$$\left|C(\varphi)\right|^2=\exp\left(-\varphi^2d^2/16\pi^2\right) \qquad (7)$$

Hence this phenomenon observed in the as-prepared nanocrystals can be attributed to quantum confinement effect at the nanometre scale [46].

3.4. Thermal Stability Analysis

The results of thermal analysis are presented in figure 4c and in Table 2.

All the samples show small mass losses of about 20 wt. %, due to its high thermal stability. The first mass loss step could be assigned to the elimination of water and gases adsorbed on the surface of the powder. The mass loss at such low temperatures is an indication that water was adsorbed on the surface of the powder which is not attributed to the structural water. Table 2, indicates that in the temperature range of ~250ºC and 800ºC, the total mass loss for sample CuO-1.5 lost was 21.91 wt. %, CuO-2.0 was 17.73 wt.% and CuO-2.5 was 16.71 wt. %. This indicates that the percentage thermal weight loss decreases with increasing NaOH concentration and decreasing crystalline domain size consistent with the observations in the XRD data analysis.

Table 2. Data from thermal analysis of the CuO nanocrystals

Sample	Step	Temp. (ºC).	Mass loss (%)	Mass loss (mg)	Res. Mass (mg)	Residual Mass (%)
CuO - 1.5	1	26.98-208.20	6.08	0.67	10.27	85.34
	2	208.20-282.68	7.44	0.82	9.45	84.67
	3	282.68-337.12	0.67	0.074	9.37	78.87
	4	337.12-589.74	5.80	0.64	8.73	**78.09**
CuO - 2.0	1	25.02-75.29	0.41	0.04	9.80	98.50
	2	75.29-202	12.16	1.21	8.59	86.33
	3	202.25-253.97	1.32	0.13	8.46	85.02
	4	253.97-895.09	2.74	0.27	8.19	**82.27**
CuO - 2.5	1	25.0-111.04	0.73	0.08	10.17	98.27
	2	111.04-197.42	7.021	0.73	9.44	91.25
	3	197.42-258.19	1.85	0.19	9.25	89.40
	4	258.19-403.23	4.19	0.43	8.82	85.21
	5	403.23-535.08	1.92	0.20	8.62	**83.29**

3.5. Electrochemical Analysis

To investigate the electrochemical behaviour of the as-prepared CuO leaf-like nanostructures as potential electrode material for electrochemical capacitors, cyclic voltammetry studies were performed on the samples. Figure 5 shows the CV curves of the three CuO samples measured at different scan rates of 10 mV s^{-1}, 25 mV s^{-1}, 50 mV s^{-1} and 75 mV s^{-1} in 2 M KOH aqueous solution. Electrochemical redox peaks are observed in the potential range from 0.1 V to 0.4 V. As observed, the CV current response of sample increases gradually with increasing scan rate, indicating reversible redox reaction taking place at the electrode material interface: all CVs show typical pseudocapacitance behaviour. Results also show two main peaks, a broad cathodic peak, and anodic peaks corresponding to redox peak of Cu^{2+}/Cu. Storage mechanism in CuO have been proposed as follows. It is based on the intercalation/extraction of protons in the electrode that is oxidation/reduction of the electrode (surface adsorption and desorption of protons). When the CuO electrode is swept towards a negative potential, cathodic current flows according to $Cu^{2+} \leftrightarrow Cu^{+1}$ reduction process while during a positive potential sweep, anodic

current flows due to $Cu^{1+} \leftrightarrow Cu^{2+}$ oxidation process. The net redox reaction can be represented by equation 8.

$$Cu^{2+} + e^{-} \leftrightarrow Cu^{+} \quad (8)$$

The ratio of the anodic to cathodic peak current (I_{pa}/I_{pc}) is approximately unity, indicating the redox reaction of CuO nanoparticles is a reversible process.

The gravimetric capacitance of the electrodes was calculated graphically by integrating the area of the cyclic voltammetry curve using the following equation [47]:

$$C_s = \frac{i}{vw} \quad (9)$$

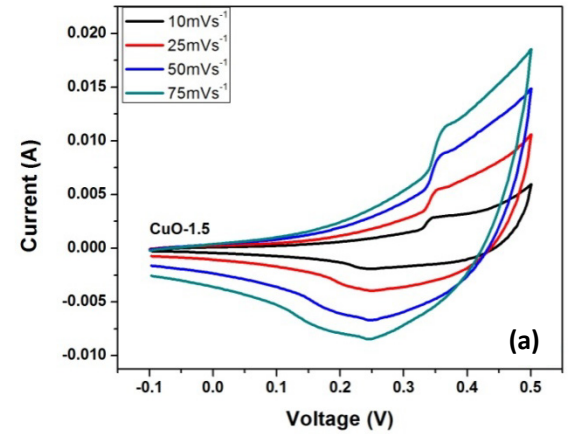

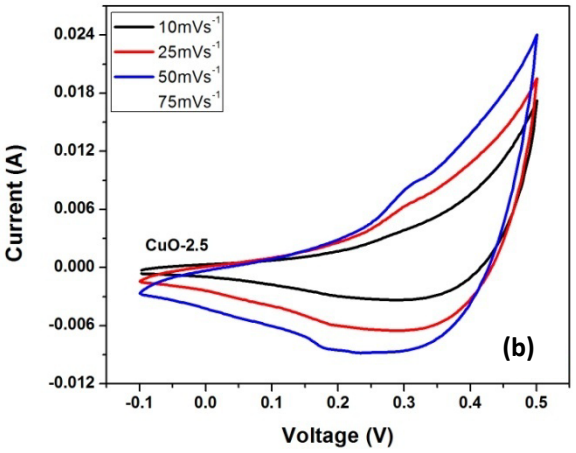

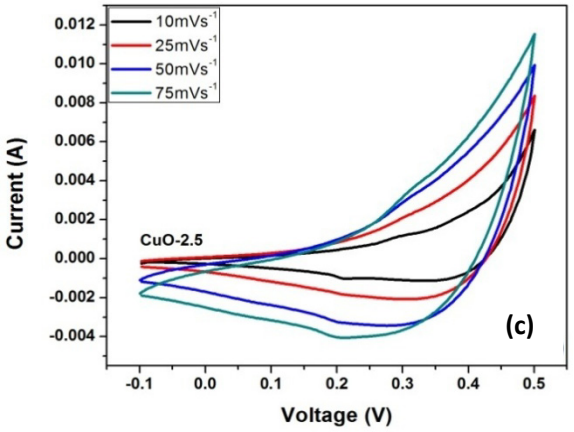

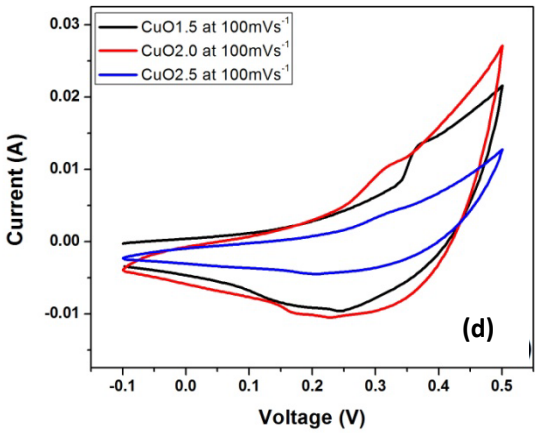

Figure 5. CV curves measured at different scan rates of 10 mV s^{-1}, 25 mV s^{-1}, 50 mV s^{-1} and 75 mV s^{-1} in 2 M KOH aqueous solution

Where *Cs* is the gravimetric capacitance, *w (g)* is the mass of CuO, ν is the scan rate, i is the average current measured in ampere (A).

A gravimetric capacitance value of 45.3 F g^{-1}, 42.2 F g^{-1} and 40 F g^{-1} were obtained at a scan rate of 5 mV s^{-1} for the three different electrodes. These values can be compared with previous reported values on CuO electrodes [11]. It also demonstrates that CuO has the potential application as a pseudocapacitor.

EIS is an excellent tool used to investigate the electrochemical characteristics of electrode/electrolyte interface using Nyquist plot, which is a representation of the real and imaginary part of the impedance spectroscopy. The main objective of the EIS experiments is to see the effect of particle size on the interfacial properties electrodes made from the different concentration of CuO samples (capacitance and electron charge transfer resistance).

The Nyquist plot of the three prepared electrodes is shown in figure 6.

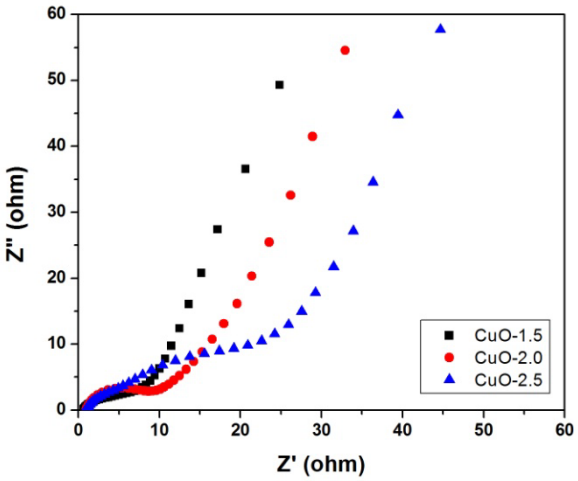

Figure 6. Nyquist plot of the CuO based electrodes

The Nyquist plot typically consists of a partial semicircle in the high-frequency region corresponding to the electron

charge transfer resistance due to the Faradaic redox process at the electrode/electrolyte interface. This resistance is associated with two resistances: electrolyte resistance and the material (oxide) resistance which arises from the non-uniform continuity in the charge transfer process at the electrode/electrolyte interface because of the differences in conductivity between the oxide (CuO) and the electrolyte [48]. A line is observed in the low-frequency region corresponding to electron-transfer diffusion process. It is worth stating that for ideal electrochemical capacitors, the (Nyquist) plot should be a line perpendicular to the real axis at low frequency region. However, there are deviation from the ideal behaviour is ascribed to the pseudocapacitance properties of the oxide material (CuO).

From the SEM and TEM Micrographs it can be observed that all the three CuO samples show similar leaf-like structure. In spite of these similar shapes, there is significant differences in charge propagation at the electrode interface during the electrochemical process which is evident by the different diameter semicircles in the Nyquist plot. That is, the diameter of the semicircles increases with increasing concentration of NaOH in the samples. From the figure, it observed that the sample with the largest semicircle has the least resistance value. The charge transfer resistance of the samples are in the following order: CuO-2.5 (0.6 Ω) < CuO-2.0 (0.84 Ω) < CuO-1.5 (0.92 Ω). A low charge transfer resistance implies a better electrochemical performance. This is in good agreement with data obtained from XRD exhibiting smaller size distributions. The results obtained here demonstrate that smaller particles have easy accessibility and mobility to OH^- ions from the electrolyte therefore having least resistance values.

4. Conclusions

Thermally mediated micellar microemulsion method has been employed to produce copper oxide (CuO) nano-leaf like structures using copper dodecyl sulphate ($Cu(DS)_2$) as precursor and varying concentrations of sodium hydroxide (NaOH) for possible applications in electrochemical capacitors. XRD analysis using the whole powder pattern modelling routine reveals that the crystalline domain size (12 nm-18 nm) and lognormal size distribution decreases with increasing concentration of NaOH. The morphologies of the nanoleaf-like structures which are believed to consist of spherical particles aligned along rods have been studied via TEM and SEM. ATR-FTIR and Raman spectroscopic investigations coupled with XRD confirm the synthesis of the monoclinic CuO nanocrystals. The broadening effects observed via these characterisation techniques are consistent with nanometre scale particle size related to quantum confinement effect. A similar nano-grain size phenomenon was observed in the thermogravimetry analysis. Impedance spectroscopy analysis also shows that samples with highest concentration of NaOH have the least (~ 0.6 Ω) charge transfer resistance. This electrochemical performance can be attributed to the small particle size distribution resulting in a high surface to volume ratio. Thus this synthesis technique could be a promising approach for production of oxide nanostructures with small domain for energy storage applications.

ACKNOWLEDGEMENTS

This work is based upon research supported by the South African Research Chairs Initiative of the Department of Science and Technology (DST) and the National Research Foundation (NRF). B. A. and DDA acknowledge the financial support from the University of Pretoria and NRF.

REFERENCES

[1] Kamimura, H., Ushio H., Matsuno S., Hamada T., 2005, Theory of copper oxide superconductors. Springer-Verlag Berlin Heidelberg.

[2] Bednorz J., Muller K., 1988, Perovskite-type oxides: the new approach to high-Tc superconductivity. Rev. of Mod. Phys. 60, 585-600.

[3] Tunell G., Posnjak E., Ksanda C.J., 1935, Geometrical and optical properties, and crystal structure of tenorite: Zeits. Kristallogr. 90,120-42.

[4] Åsbrink S., Norrby L.J., 1970, A refinement of the crystal structure of copper(II) oxide with a discussion of some exceptional e.s.d.'s. Acta Crystallographica Section B Structural Crystallography and Crystal Chemistry. 26, 8-15.

[5] Zhang J., Liu J., Peng Q., Wang X., Li Y., 2006, Nearly monodisperse Cu_2O and CuO nanospheres: preparation and applications for sensitive gas sensors. Chemistry of Materials. 18, 867-871.

[6] Wang J., He S., Li Z., Jing X., Zhang M., Jiang Z., 2009, Microemulsion synthesis of copper oxide nanorod-like structures, Colloid and Polymer Science. 287, 853-858.

[7] Shaikh J.S., Pawar R.C., Moholkar A.V., Kim J.H., Patil P.S., 2011, CuO-PAA hybrid films: chemical synthesis and supercapacitor behaviour. Applied Surface Science. 257, 4389-4397.

[8] Xiang J.Y., Tu J.P., Zhang L., Zhou Y., Wang X. L., Shi S.J., 2010, Self-assembled synthesis of hierarchical nanostructured CuO with various morphologies and their application as anodes for lithium ion batteries. Journal of Power Sources. 195,313-319.

[9] Wang S.Q., Zhang J.Y., Chen C.H., 2007, CuO-PAA hybrid films: Chemical synthesis and supercapacitor behaviour. Scripta Materialia. 57, 337-340.

[10] Xiang JY, Tu JP, Yuan YF, Wang XL, Huang XH, Zeng ZY (2009) Electrochemical investigation on nanoflower-like CuO/Ni composite film as anode for lithium ion batteries. Electrochimica Acta. 54: 1160-1165.

[11] Patake V.D., Joshi S.S., Lokhande C. D, Joo O. S., 2009,

Electrodeposited porous and amorphous copper oxide film for application in supercapacitor. Materials Chemistry and Physics. 114, 6-9.

[12] Cheng L., Shao M., Chen D., Zhang Y., 2010, Preparation, characterization, and electrochemical application of mesoporous copper oxide. Mat. Res. Bull. 45, 235-239.

[13] Song X., Yu H., Sun S., 2005, Single-crystalline CuO nanobelts fabricated by a convenient route. Journal of Colloid and Interface Science. 289, 588-591.

[14] Jisen W., Jinkai Y., Jinquan S., Ying B., 2004, Synthesis of copper oxide nanomaterials and the growth mechanism of copper oxide nanorods. Materials & Design. 25, 625.

[15] Cao M, Hu C, Wang Y, Guo Y, Guo , Wang E (2003) A controllable synthetic route to Cu, Cu_2O, and CuO nanotubes and nanorods. Chem Comm. 1:1884-1885.

[16] Yao W.T., Yu S.H., Zhou Y., Jiang J., Wu Q.S., Zhang L., et al., 2005, Formation of uniform CuO nanorods by spontaneous aggregation: selective synthesis of CuO, Cu_2O, and Cu nanoparticles by a solid-liquid phase arc discharge process. J. Phys Chem. B. 109, 14011.

[17] Du G., Tendeloo G.V., 2004, $Cu(OH)_2$ nanowires, CuO nanowires and CuO nanobelts, Chem. Phy Lett. 393,64.

[18] Huang L. S., Yang S.G., Li T., Gu B.X., Du Y.W., Lu Y.N., et al, 2004, Preparation of large-scale cupric oxide nanowires by thermal evaporation method. Journal of Crystal Growth. 260, 130.

[19] Liu B., Zeng H. C., 2004, Mesoscale organization of CuO nanoribbons: formation of dandelions. J Am Chem Soc. 126,8124.

[20] Chang Y., Zeng H.C., 2004, Controlled synthesis and self-assembly of single-crystalline CuO nanorods and nanoribbons. Crystal Growth & Design. 4:397-402.

[21] Zarate R.A., Hevia F., Fuentes S., Fuenzalida V.M., Zúñiga A., 2007, A. Novel route to synthesize CuO nanoplatelets. Journal of Solid State Chemistry. 180,1464.

[22] Wang H., Shen Q., Li X., Liu F., 2009, Fabrication of copper oxide dumbbell-like architectures via the hydrophobic interaction of adsorbed hydrocarbon chains. ACS Journal of Surfaces and Colloids. 25, 3152.

[23] Kumar R., Diamant Y., Gedanken, 2000, A Sonochemical synthesis and characterization of nanometer-size transition metal oxides from metal acetates, Chem Mater. 12, 2301.

[24] Hsieh C.T., Chen J.M., Lin H.H., Shih H.C., 2003, Synthesis of well-ordered CuO nanofibers by a self-catalytic growth mechanism. Appl. Phy. Lett. 82, 3316.

[25] Barreca D., Comini E., Gasparotto A., Maccato C., Sada C., Sberveglieri G., et al., 2009, Chemical vapor deposition of copper oxide films and entangled quasi-1D nanoarchitectures as innovative gas sensors. Sensors and Actuators B: Chemical. 141, 270.

[26] Lee S., Her Y., Matijevi E., 1997, Preparation and growth mechanism of uniform colloidal copper oxide by the controlled double-jet precipitation. Journal of Colloid and Interface Science. 186,193.

[27] Dodoo-Arhin D., Leoni M., Scardi P., 2012, Microemulsion synthesis of copper oxide nanorod-like structures. Molecular Crystals and Liquid Crystals. 555,17.

[28] Liu B., Zeng H.C., 2004, Fabrication of ZnO Dandelions via a modified Kirkendall process. J Am. Chem. Soc. 126, 16744.

[29] Scardi P., Leoni M., 2002, Whole powder pattern modelling. Acta Crystallographica. A58, 190.

[30] Caglioti G., Paoletti A., Ricci F., 1958, Choice of collimators for a crystal spectrometer for neutron diffraction. Nuclear Instruments. 3, 223.

[31] Leoni M, Confente T, Scardi P (2006) A flexible program implementing Whole Powder Pattern Modelling. Zeitschrift Für Kristallographie 249.

[32] Iino T., Ohashi K., Mune Y., Inokuchi Y., Judai K., Nishi N., et al., 2006, Infrared photodissociation spectra and solvation structures of $Cu^+(H_2O)n$ (n = 1–4). Chem Phy Lett. 427, 24.

[33] Chen Q., Shen X., Gao H., 2007, Formation of nanoparticles in water-in-oil microemulsions controlled by the yield of hydrated electron: The controlled reduction of Cu^{2+}. Journal of Colloid and Interface Science. 308,491.

[34] Li W., Shi E., Zhong W., Yin Z., 1999, Growth mechanism and growth habit of oxide crystals. Journal of Crystal Growth. 203,186.

[35] Li W., Gao L., Guo J. K., 1998, Synthesis of yttria-stabilized zirconia nanoparticles by heating of alcohol-aqueous salt solutions. Nanostructured Materials. 10, 1043-1049.

[36] Anandan S., Wen X., Yang S., 2005, Room temperature growth of CuO nanorod arrays on copper and their application as a cathode in dye-sensitized solar cells. J.Mat. Chem. phys. 93, 35-40.

[37] Cano H., Gabas N., Canselier J.P., 2001, Experimental study on the ibuprofen crystal growth morphology in solution. J. Cryst. Growth 224,335-341.

[38] Sun Y., Xia Y., 2002, Large-Scale Synthesis of Uniform Silver Nanowires Through a Soft, Self-Seeding, Polyol Process, Adv. Mater., 14,833–837.

[39] Oswald H.R., Reiler A., Schmalle H.W., Dubler F., 1990, Structure of copper(II) hydroxide. Acta Crystallogr. C 46, 2279-2284.

[40] Weller H., Schmidt H. M., Koch U., Fojtik A., Baral S., Henglein A., Kunath W., Weiss K., Dieman E., 1986, Photochemistry of colloidal semiconductors: Onset of light absorption as a function of size of extremely small CdS particles. Chem. Phys. Lett. 124, 557-560.

[41] Wu H., Lodi S., Morbidelli M., 2002, Characterization of Particle Interaction Energy through Incipient Turbulent Aggregation. J Col. Inter.Sci. 256,304.

[42] Kliche G., Popovic Z., 1990, Far-infrared spectroscopic investigations on CuO. Phys Rev B. 42, 10060–10066.

[43] Xu Y., Chen D., Jiao X., 2005, Fabrication of CuO Pricky Microspheres with Tunable Size by a Simple Solution Route. J Phys Chem. B. 109, 13561–13566.

[44] Goldstein H., Kim D., Yu P., 1990, Raman study of CuO single crystals. Phys Rev B. 41, 192–7194.

[45] Chrzanowski J., Irwin J., 1989, Raman scattering from cupric

oxide. Solid State Comm. 70, 1, 11–14.

[46] Yang J., Meldrum F.C., Fendler J.H., 1995, Epitaxial-growth of size-quantized cadmium-sulfide crystals under arachidic acid monolayers, J phys chem. 99 (15), 5500-5504.

[47] Shaikh J.S., Pawar R.C., Mali S.S., Moholkar A.V., Kim J.H., Patil P.S., 2010, Effect of annealing on the supercapacitor performance of CuO-PAA/CNT films. J Sol State Electrochem. 16(1), 25-33.

[48] Meher S.K., Justin P., Rao G.R., 2011, Microwave-mediated synthesis for improved morphology and pseudocapacitance performance of nickel oxide. ACS Applied Materials & Interfaces. 3,2063.